J Therm Anal Calorim (2012) 109:1185–1191
DOI 10.1007/s10973-012-2370-y

# The effect of cooling rate on the solidification and microstructure evolution in duplex stainless steel

## A DSC study

**Darja Steiner Petrovič · Miran Pirnat · Grega Klančnik · Primož Mrvar · Jožef Medved**

NATAS2011 Conference Special Chapter


**Abstract** The effects of the cooling rate on the solidification and microstructure evolution in the duplex stainless steel SAF 2205 was studied using DSC and light microscopy. A ferritoscope was used to measure the ferrite content. It was revealed that the cooling rate has an influence on the $\delta$-ferrite nucleation temperature and the width of the solidification interval. Moreover, with an increase in cooling rate, the content of $\delta$-ferrite increases, while the quantity of austenite in the ferrite matrix decreases and its morphology changes to acicular. A two-cycle DSC experiment made possible a more accurate interpretation of the collected data.

**Keywords** DSC · Duplex stainless steel · Solidification · Cooling rate · Precipitation

## Introduction

Duplex stainless steels (DSSs), i.e., those with a mixed microstructure containing approximately equal proportions of austenite and ferrite, have existed for nearly 80 years [1]. These DSSs have both an excellent corrosion resistance and good mechanical properties, as a consequence of their two-phase microstructure, i.e., the tough austenite ($\gamma$) and the harder ferrite ($\delta$) [1–3].

The first generation of DSSs had limitations in the as-welded condition. The heat-affected zone (HAZ) of the welds had a low toughness because of the excessive ferrite and the significantly lower corrosion resistance than that of the base metal. The second-generation DSSs are defined by their nitrogen alloying. This nitrogen alloying improves the HAZ's toughness and the corrosion resistance. Moreover, with the increased austenite stability, the nitrogen also reduces the rate at which detrimental intermetallic phases form [1]. Besides, a refinement of the matrix grains and a uniform distribution of the fine, secondary phases are essential in order to improve their mechanical properties [2].

DSSs have a very good hot-cracking resistance due to their high ferrite content [4]. The problems of most concern in DSSs are associated with the HAZ, not with the weld metal [1].

One of the aspects that play an important role is the solidification rate. The cooling rate is normally not uniform during the solidification of the steel, e.g., in continuous casting or welding. It is reported that the cracking of DSSs depends on the ferrite/austenite ratio during the solidification process of the steel [5].

The properties of DSSs depend not only on the ferrite/austenite ratio but also to a large extent on the precipitation of secondary phases, such as the sigma phase ($\sigma$), chromium nitrides (CrN, $Cr_2N$,) and the chi phase ($\chi$). The temperature range of precipitation for each phase depends on the steel's chemical composition, the solidification conditions, and the thermomechanical treatment [3]. Also, the difference in the diffusibilities of chromium and

**Electronic supplementary material** The online version of this article (doi:10.1007/s10973-012-2370-y) contains supplementary material, which is available to authorized users.

D. Steiner Petrovič (✉)
Institute of Metals and Technology, Ljubljana, Slovenia
e-mail: darja.steiner@imt.si

M. Pirnat
Acroni, d.o.o, Jesenice, Slovenia

G. Klančnik · P. Mrvar · J. Medved
Faculty of Natural Sciences and Engineering,
University of Ljubljana, Ljubljana, Slovenia

nitrogen in the delta ferrite during cooling may influence the precipitation of chromium nitrides [6]. It is well known that the solidification rate influences the size and morphology of the microstructural constituents [7–9].

The aim of our investigation was to determine the effect of the cooling rate on the solidification of DSS using differential scanning calorimetry (DSC). DSC is frequently applied to study the reaction and transformation kinetics of steels [10, 11].

In this study, DSC experiments were performed in two consecutive cycles. It is reported [12] that multicycle DSC can be used to search for weak or even hitherto undetected caloric transitions for their qualitative or quantitative elucidation.

## Experimental

The alloy used in this study was the DSS SAF 2205. This alloy is a 21.0–23.0% Cr, 2.5–3.5% Mo, 4.5–6.5% Ni, nitrogen-alloyed DSS.

Specimens for the thermal analysis were taken from hot-rolled plates.

The final chemical composition of the steel specimens is listed in Table 1.

The thermal analysis was performed using DSC in a STA-449 C Jupiter, Netzsch instrument. The dynamic measurements involved two consecutive cycles at the same selected ramp rates. First, the furnace was linearly heated above the liquidus temperature to 1,550 °C at heating rates of 5, 10, and 25 K/min. Then, the solidification scans from 1,550 °C at the same cooling ramps were performed. Two cycles were used to eliminate the effects of the as-received microstructure and to achieve a better contact in the DSC experiments.

The liquidus temperature was estimated assuming the fact that the determination of liquidus temperature using DSC heating curve is strongly mass dependent. It is customary to select the peak temperature of the last thermal event on heating as the liquidus temperature [13]. Accordingly, the ferrite nucleation was determined as first temperature recorded on the cooling curve. The solidification interval was defined as the difference between the average nucleation temperature and average solidus temperature determined on the first and second cooling. The tangents construction for the solidus temperature was done on the DSC cooling curve with the extrapolation of the peaks slope down to a baseline. Because this determination is also mass dependent rather similar loads were taken for all three cooling rates. The approximate specimen dimensions were $3 \times 3 \times 3$ mm$^3$, with the specimen weighing approximately 200 mg.

The DSC experiments were conducted under a static atmosphere of nitrogen with 99.999 vol% purity to prevent both the denitrogenation of the steel and to minimize the surface oxidation. An empty corundum crucible was taken as a reference. For the purposes of this study, the DSC signal was evaluated.

The solidification sequence of the DSS and the precipitation of the secondary phases were also predicted with thermodynamic calculations using ThermoCalc-TCW5.

Following the DSC measurements, the specimens were metallographically analyzed. A Nikon Microphot FXA optical microscope equipped with a Hitachi HV-C20AMP 3CCD video camera and a Fischer MP30 ferritoscope were used in the metallographic examinations.

The ferritoscope operates by generating an alternating magnetic field in the specimen which is proportional to the ferrite content and which the instrument can detect. The instrument measures the relative permeability of the material in the alternating magnetic field of its probe.

## Results and discussion

### Thermodynamic calculations

The thermodynamic calculations were performed with TCW5 for the prediction of the solidification process of the selected DSS SAF 2205.

The phase equilibria were calculated in the temperature range 400–1,600 °C. Figure 1 presents the volume fraction ($\Phi_i$) of the equilibrium phases in the selected temperature range. In this study, the lowest temperature of thermodynamic calculations (i.e., 400 °C) was selected according to the classic approach, which takes into account only the temperatures of the effective diffusion.

According to the equilibrium phase diagram presented in Fig. 1, the selected SAF 2205 steel solidifies with the primary formation of $\delta$-ferrite, which has a b.c.c. crystallographic structure. The primary formed $\delta$-ferrite transforms into a $\gamma$-phase, an austenite with the f.c.c. crystallographic structure. With a decreasing temperature, and under equilibrium solidification conditions, the precipitation of secondary phases, such as the chromium

**Table 1** Chemical composition and some characteristics of the DSS SAF 2205 used in the present investigation/mass%

| | %C | %Si | %Mn | %Cr | %Ni | %Mo | %N | $Cr_{eq.}$ | $Ni_{eq.}$ | $Cr_{eq.}/N_{eq.}$ | FN |
|---|---|---|---|---|---|---|---|---|---|---|---|
| SAF 2205 | 0.024 | 0.49 | 1.4 | 22.41 | 5.31 | 3.13 | 0.165 | 26.29 | 11.78 | 2.232 | 36.49 |

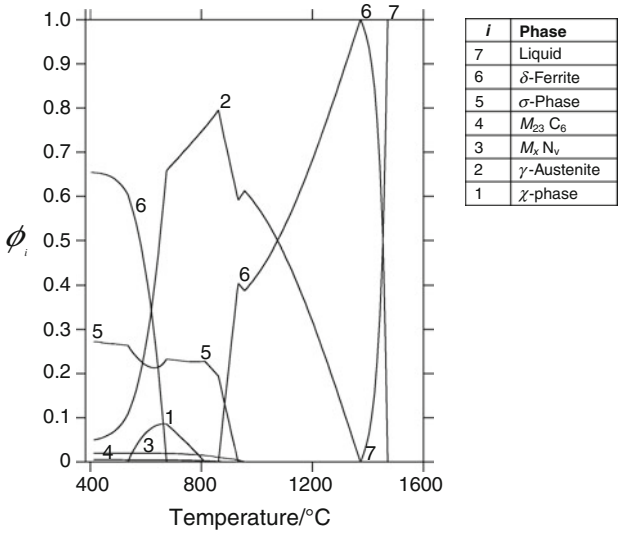


**Fig. 1** Volume fraction of equilibrium phases as a function of temperature for the selected DSS SAF 2205 with the chemical composition given in Table 1

nitrides $Cr_xN$, the $M_{23}C_6$ carbides, the sigma phase ($\sigma$), and the chi phase ($\chi$), will proceed.

According to the thermodynamic calculations for this specific DSS, the phase transformation from $\delta$-ferrite to austenite takes place below 1,325 °C (Fig. 1). The calculated volume fractions of the equilibrium phases at 1,074 °C are 50% of $\delta$-ferrite and 50% $\gamma$-phase. On the other hand, at 400 °C the volume fractions of the calculated equilibrium phases are: 63.5% $\delta$-ferrite, 27.6% $\sigma$-phase, 5% $\gamma$-phase, 2% $Cr_xN$, and <1% $M_{23}C_6$. Nevertheless, with decreasing temperature the amount of precipitated phases depends on both, the diffusion and precipitation kinetics.

## Differential scanning calorimetry

The steel specimens were heated above the liquidus temperature to enable monitoring of their solidification behavior while cooling down.

Linear heating and cooling at selected ramp rates (5, 10, and 25 K/min) was repeated in two consecutive cycles. The melting reactions obtained using DSC were characterized by several endothermic peaks, whereas the cooling reactions were characterized by the presence of several exothermic peaks.

During the second cycle of melting and solidification at the slowest cooling rate (5 K/min), two peaks could be easily identified between the solidus and liquidus temperature in the corresponding DSC curves (see Figs. 2, 4). The reaction sequence between the solidus and liquidus temperature was not so clearly expressed with the other two ramp rates, i.e., 10 and 25 K/min.

Therefore, a more detailed explanation of the reaction sequence will be given using the DSC curves obtained at 5 K/min.

## Melting curves

### *First cycle*

The typical DSC melting curve obtained at a heating rate of 5 K/min is characterized by sequential melting, as confirmed by several endothermic peaks.

It is assumed that the endothermic peak involving 2.821 J/g of reaction enthalpy with a $T_{onset}$ at about 485 °C represents the dissolving of chromium-rich $\alpha'$-phase [14]. The next endothermic peak involving 37.83 J/g of enthalpy with a $T_{onset}$ at about 818 °C can be ascribed to the transformation of tertiary austenite ($\gamma_3$) into ferrite and the dissolving of precipitates, e.g., carbides, nitrides, $\chi$-phase, and $\sigma$-phase [14, 15]. At $T = 1119.6$ °C, the endothermic peak involving 77.95 J/g of reaction enthalpy can be associated with the solid-state transformation of secondary austenite into ferrite $\gamma_2 \rightarrow \delta$ [14]. The $T_{onset}$ of the major endothermic reaction(s) is around 1,407 °C related to the melting of the last solidified metal melt and with the disappearance of ferrite. The(se) endothermic reaction(s) evolved 41.17 J/g of enthalpy.

### *Second cycle*

The second cycle DSC melting curve was obtained after heating and cooling the specimen at the selected ramp rate (Fig. 2).

Here, the endothermic peak involving 3.526 J/g of reaction enthalpy with a $T_{onset}$ at about 448 °C represents dissolving of chromium-rich $\alpha'$-phase. The next endothermic peak involving 5.258 J/g of enthalpy with a $T_{onset}$ at about 706 °C can be ascribed to the transformation of $\gamma_3$ and the dissolving of precipitates (carbides, nitrides, $\chi$-phase, and $\sigma$-phase). At $T = 967.4$ °C, the endothermic peak involving 36.03 J/g of reaction enthalpy can be associated phase transformation $\gamma_2 \rightarrow \delta$. The $T_{onset}$ of the major endothermic reaction(s) is 1412.4 °C. 1412.4 °C represents the solidus temperature. Above the solidus temperature, the melting proceeds. Here, two endothermic peaks can be clearly seen. The first peak may be associated with the crystal segregations [14]. Above 1428 °C, the melting of $\delta$-ferrite proceeds. These endothermic reactions evolved 55.32 J/g of enthalpy. It can be seen in Fig. 2 that some effects arising from an industrial technological process are minimized. Namely, the microstructural evolution during industrial processing has an effect on the anisotropy of the final industrial product [16].

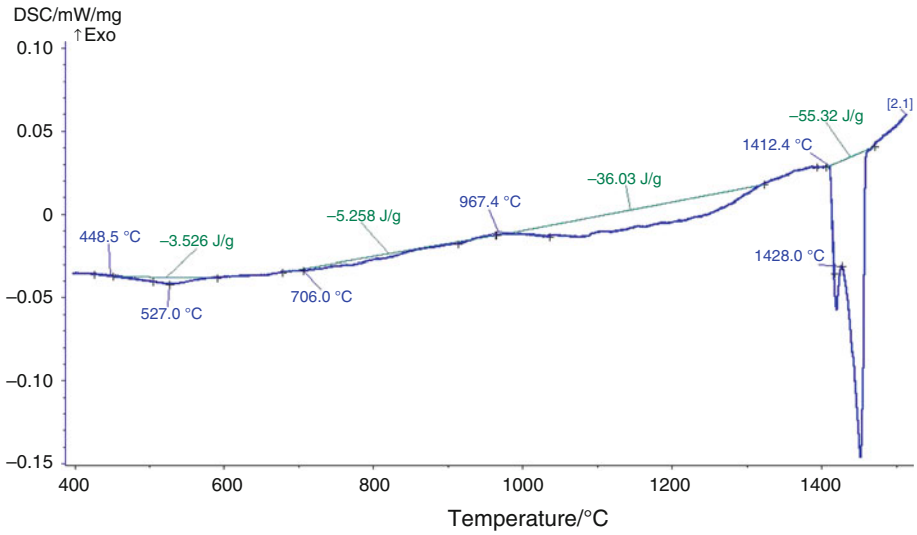


**Fig. 2** Melting curve of the SAF 2205, second cycle (static nitrogen atmosphere; heating rate 5 K/min)

## Solidification curves

DSC solidification curves can be used to interpret the solidification mechanisms, so we compared the exothermic peaks evolved during the cooling. The details for the first cycle experiments are shown in Fig. 3.

The width of the solidification interval increased with the increasing cooling rate. The highest recorded temperature related with the solidification of primary ferrite was measured at the slowest cooling rate (1450.7 and 1451.1 °C at 5 K/min) and, vice versa, the lower temperatures were measured at faster cooling rates (1444.0 and 1447.0 °C at 10 and 25 K/min, respectively).

The recorded temperatures of ferrite formation from the melt during cooling were not identical for the three scan rates, demonstrating that the cooling rate has a significant effect on the solidification reactions due to non-equilibrium conditions.

As mentioned earlier, during the second cycle of melting and solidification at 5 K/min, the reaction sequence was clearly evidenced in the corresponding DSC curves. Therefore, the obtained DSC cooling curves at a cooling rate of 5 K/min will be used for a more detailed explanation.

### *First cycle*

In the DSC cooling curve obtained at 5 K/min, the major exothermic peak involving 58.5 J/g of reaction enthalpy with a $T_{onset}$ at about 1,450 °C represents the precipitation of primary $\delta$-ferrite from the melt. The next exothermic peaks of lower intensities at 1374, 1136, and 1058 °C can be ascribed to the $\delta \rightarrow \gamma$ transformations, and the precipitation of thermodynamically stable secondary phases, e.g., the $\sigma$-phase, $\chi$-phase, CrN, $Cr_2N$, carbides [11, 14, 15]. Nevertheless, the weak thermal effects determined for the

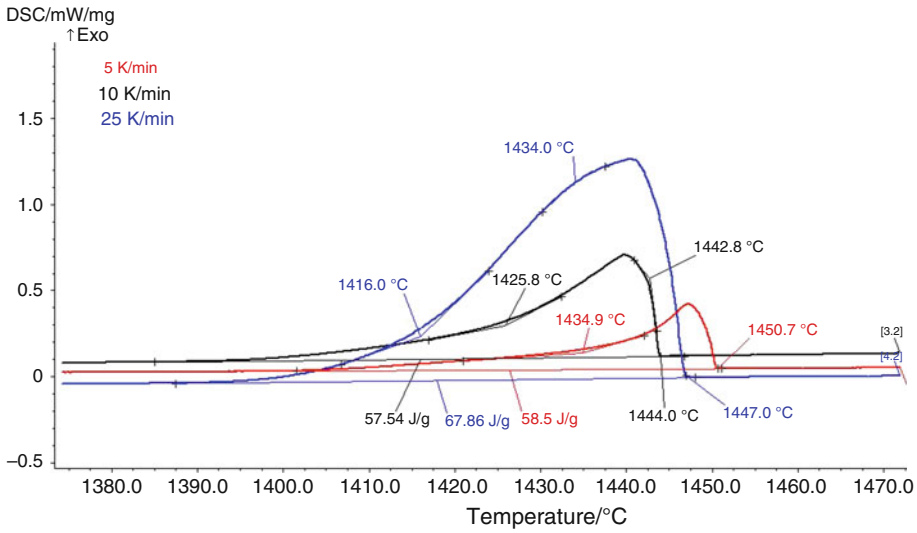


**Fig. 3** Details of the DSC solidification curves for SAF 2205 obtained at various cooling rates (5, 10, and 25 K/min, first cycle)

solid–solid transformations, as also precipitations, is confirmed by the fact that the microstructure is mainly composed from ferrite and austenite.

*Second cycle*

The reaction sequence between solidus and nucleation temperature could only be evidenced by detecting two peaks in the second cycle of the DSC cooling run obtained at 5 K/min as shown in Fig. 4.

The major exothermic reactions involved 60.16 J/g of reaction enthalpy. The $T_{onset}$ of the primary reaction described by $L \rightarrow L + \delta$ was at 1451.1 °C. The second exothermic peak in the cooling curve may be associated with the eutectic reaction $L \rightarrow \delta + \gamma_1$ [14]. The phase transformation of the $\delta$-ferrite to $\gamma_2$ begins at 1,388 °C. This is also in good agreement with the thermodynamic calculations presented in Fig. 1. The next exothermic peaks of lower intensities were detected at 1,124 and 1,003 °C. They can be ascribed to the precipitation of thermodynamically stable secondary phases [11, 14, 15].

From a comparison of the first and second cycles of the DSC experiments, the influence of industrial conditions on the solidification process and the precipitation of secondary phases can be seen.

Furthermore, using two consecutive DSC cycles, the liquidus, solidus, and nucleation temperatures could be determined more precisely. The experimental data are collected in Table 2.

From the experimental data, some trends related to the cooling rate could be assessed. During solidification, with an increasing cooling rate, the liquidus temperature decreases. If the differences between the average values of the estimated solidus and nucleation temperatures are taken into account, it can be concluded that the width of the solidification interval increased with the increasing cooling rate.

Using the two-cycle DSC when studying the solidification phenomena means the sensitivity of the experiment can be improved due to the possibility of a more accurate interpretation of the collected data.

## Metallography

Figure 5 shows the as-solidified microstructures of SAF 2205 solidified at different cooling rates. Micrographs were taken at magnifications of ×50 to ×200. It can be seen that the microstructures consist of both $\delta$-ferrite and austenite phases.

It was observed that with the increasing cooling rate, the quantity of precipitated austenite in the ferrite matrix decreases and its morphology changes to acicular. In addition, the structure of the precipitated austenite refines.

As a result of the increased cooling rate, a varying solute concentration ahead of the solidification front may appear. The possible segregation of solutes may cause the constitutional supercooling of the liquid [14, 17].

Besides the observed variations in the microstructure morphology, there can also be a corresponding variation of the liquidus temperature, as can be seen in Table 2.

Under equilibrium solidification conditions, the $\delta$-ferrite would transform into an austenite in the temperature range from 1,325 °C to approximately 900 °C. The time of holding the steel in that temperature range is very important for the ferrite/austenite ratio in the as-solidified microstructure. These results are in a good agreement with the results of Li et al. [5].

Our metallographic observations were also supported with ferritoscope measurements. The results of the content of $\delta$-ferrite in all three specimens are given in Table 3.

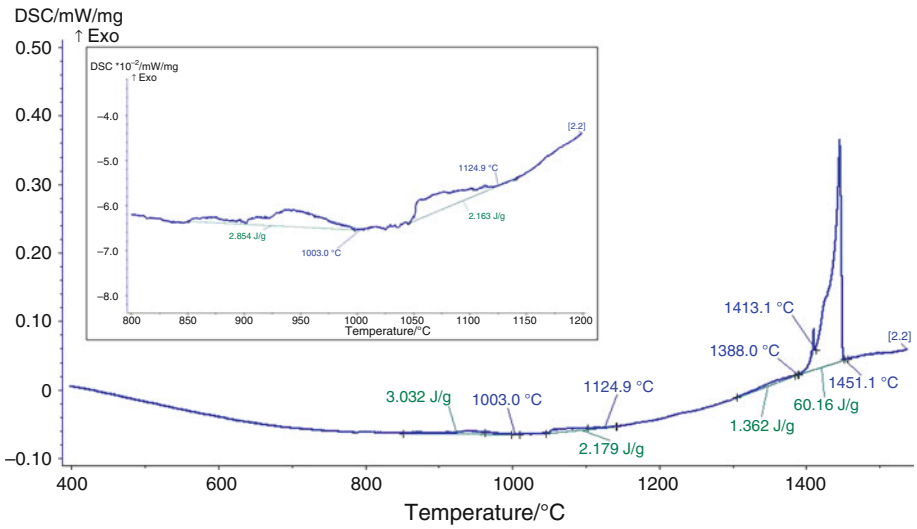


**Fig. 4** Cooling curve of the SAF 2205, second cycle (static nitrogen atmosphere; cooling rate 5 K/min)

**Table 2** Estimated solidification interval ($\Delta T$), and liquidus, solidus, and $\delta$-ferrite nucleation temperatures/°C

| | First heating | First cooling | Second heating | Second cooling | $\Delta T$/°C |
|---|---|---|---|---|---|
| 5 K/min | | | | | |
| Liquidus/°C | 1452.8 | – | 1453.3 | – | 49.55 |
| Solidus/°C | 1407.4 | 1401.7 | 1412.4 | 1401.0 | |
| Ferrite nucleation/°C | – | 1450.7 | – | 1451.1 | |
| 10 K/min | | | | | |
| Liquidus/°C | 1459.0 | – | 1457.0 | – | 49.90 |
| Solidus/°C | 1407.0 | 1395.5 | 1407.0 | 1396.7 | |
| Ferrite nucleation/°C | – | 1444.0 | – | 1448.0 | |
| 25 K/min | | | | | |
| Liquidus/°C | 1465.0 | – | 1467.0 | – | 50.85 |
| Solidus/°C | 1412.0 | 1396.2 | 1410.0 | 1396.4 | |
| Ferrite nucleation/°C | – | 1447.0 | – | 1447.3 | |

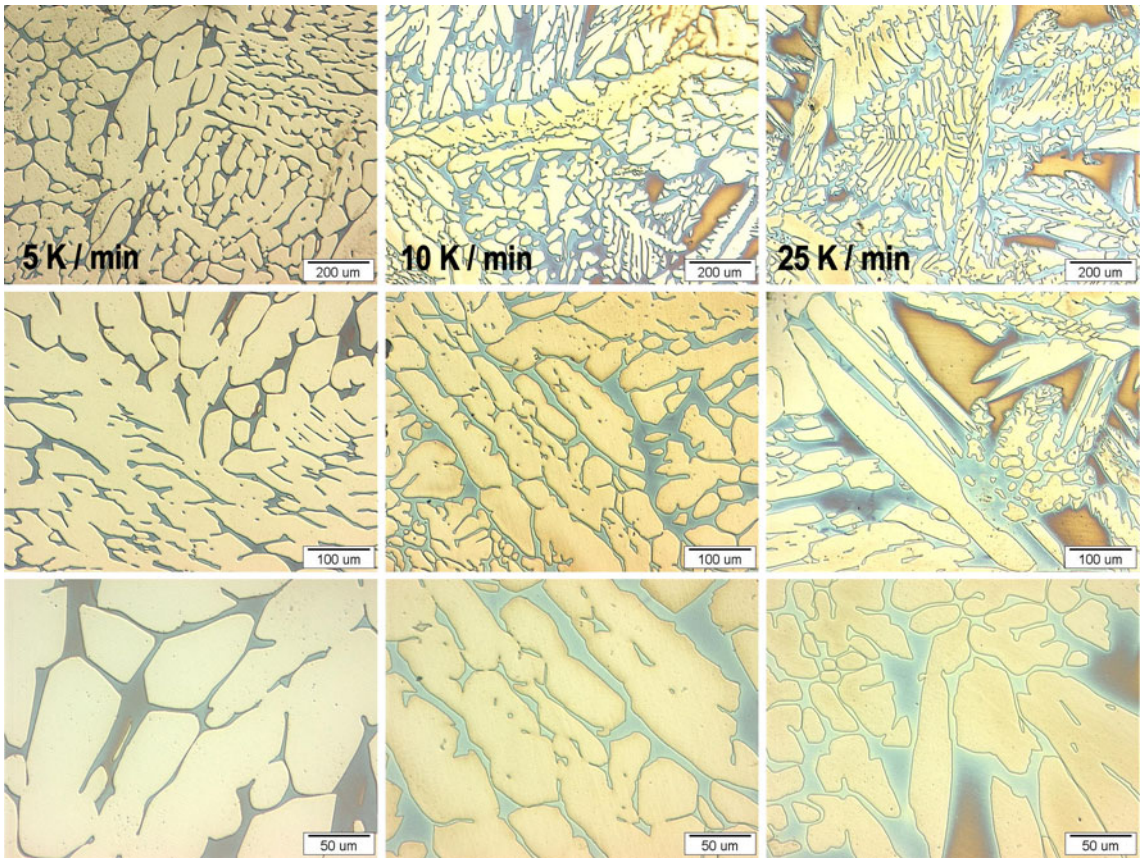


**Fig. 5** As-solidified microstructures of SAF 2205 at various cooling rates (LM: ×50, ×100, and ×200. Etchant: Murakami's)

Using light microscopy, the presence of a deleterious sigma phase ($\sigma$) was not observed in the as-solidified microstructures.

Content of the $\delta$-ferrite

The volume fraction of $\delta$-ferrite in the as-received (DU-0) and all three specimens solidified at 5, 10, and 25 K/min (DU-5, DU-10, DU-25) was determined using the ferritoscope. The results are given in Table 3.

The lowest volume fraction of $\delta$-ferrite was measured in the specimen DU-5, which was solidified at the lowest cooling rate (5 K/min). These observations are in accordance with the results of Li et al. [5].

**Table 3** Average volume fraction of $\delta$-ferrite in as-solidified specimens of the DSS SAF 2205

| | $\delta$-Ferrite/vol% | Average[a] value of $\delta$-ferrite/vol% |
|---|---|---|
| DU-0 | 42.3 | 41.8 |
| | 41.6 | |
| | 41.4 | |
| | 42.6 | |
| | 41.0 | |
| DU-5 | 13.7 | 13.5 |
| | 13.7 | |
| | 11.7 | |
| | 13.8 | |
| | 13.2 | |
| DU-10 | 22.9 | 22.9 |
| | 22.3 | |
| | 23.5 | |
| | 22.4 | |
| | 23.7 | |
| DU-25 | 30.0 | 29.2 |
| | 29.6 | |
| | 30.1 | |
| | 27.6 | |
| | 28.1 | |

[a] The highest and the lowest value were excluded from the calculation

The difference in measured values of $\delta$-ferrite in the microstructures confirms the kinetic-dependent precipitation of the $\delta$-ferrite.

## Conclusions

DSC curves of the DSS SAF 2205 clearly show the influence of the various cooling rates on the solidification sequence. The cooling rate has an influence on the liquidus temperature and the width of the solidification interval. The liquidus temperature decreases with an increasing cooling rate, whereas the width of the solidification interval increases with the increasing cooling rate.

According to the thermodynamic calculations, the selected SAF 2205 steel solidifies with the primary formation of $\delta$-ferrite, which has a b.c.c. crystallographic structure. The primary formed $\delta$-ferrite transforms into a $\gamma$-phase, an austenite with the f.c.c. crystallographic structure.

A metallographic analysis revealed that the solidification behavior, depending on the cooling rate, determines the microstructure evolution. In the microstructures of selected SAF 2205 specimens at different cooling rates, the microstructures consist of both $\delta$-ferrite and austenite phases.

With an increasing cooling rate, the content of $\delta$-ferrite increases.

With the increasing cooling rate, the quantity of precipitated austenite in the ferrite matrix decreases and its morphology changes to acicular.

Moreover, it was shown that using two-cycle DSC when studying the solidification phenomena means the sensitivity of the experiment was improved due to the possibility of a more accurate interpretation of the collected data.

**Acknowledgements** The authors would like to acknowledge Acroni d.o.o., Jesenice, Slovenia, for the supply of the steel. The study was also supported by the Slovenian Research Agency (Pr.No. P2-0050).

## References

1. Practical Guidelines for the Fabrication of Duplex Stainless steel, vol. 5, 2nd ed. London: International Molybdenum Association; 2009. p. 36.
2. Maki T, Fufuhara T, Tsuzaki K. Microstructure development by thermomechanical processing in duplex stainless steel. ISIJ Int. 2001;41:571–9.
3. Fazarinc M, Terčelj M, Bombač D, Kugler G. Transformation and precipitation kinetics in 30Cr10Ni duplex stainless steel. Metal Mater Trans A. 2010;41:2197–207.
4. Bhadeshia HKDH, Honeycombe RWK. Steels. 3rd ed. Amsterdam: Elsevier; 2007. p. 274.
5. Li Z, Zhong H, Sun Q, Xu Z, Zhai Q. Effect of cooling rate on hot-crack susceptibility of duplex stainless steel. Mater Sci Eng A. 2009;506:191–5.
6. Liao JS. Nitride precipitation in weld HAZs of duplex stainless steel. ISIJ Int. 2001;41:460–7.
7. Zupanič F, Bončina T, Križman A, Markoli B, Spaić S. Microstructural constituents of the Ni-based superalloy GMR 235 in the as-cast conditions. Scr Mater. 2002;46:667–72.
8. Liang GF, Wan CQ, Wu JC, Zhu GM, Yu Y, Fang Y. In situ observation of growth behaviour and morphology of delta-ferrite as function of solidification rate in an AISI304 stainless steel. Acta Metall Sin. 2006;19:441–8.
9. Steiner Petrovič D, Klančnik G, Pirnat M, Medved J. Differential scanning calorimetry study of the solidification of austenitic stainless steel. J Therm Anal Calorim. 2011;105:251–7.
10. Gojic M, Suceska M, Rajic M. Thermal analysis of low alloy Cr–Mo steel. J Therm Anal Calorim. 2004;75:947–56.
11. Lecomte-Beckers J, Moureaux P, Carton M, Habraken AM. Characterization of Duplex steel Uranus 76 N during deformation and heat treatment. Phys Stat Sol A. 2006;203:3651–64.
12. Marti E, Kaisersberger E, Füglein E. Multicycle differential scanning calorimetry. J Therm Anal Calorim. 2010;101:1189–97.
13. Boettinger WJ, Kattner UR, Moon KW, Perepezko JH. DTA and Heat-flux DSC measurements of alloy melting and freezing. Special publication 960-15. National Institute of Standards and Technology, Washington; 2006:35.
14. Pohl M, Storz O, Glogowski T. Effect of intermetallic precipitations on the properties of duplex stainless steel. Mater Charact. 2007;58:65–71.
15. Michalska J, Sozanska M. Qualitative and quantitative analysis of $\sigma$ and $\chi$ phases in 2205 duplex stainless steel. Mater Charact. 2006;56:355–62.
16. Fargas S, Akdut N, Anglada M, Mateo A. Microstructural evolution during industrial rolling of duplex stainless steel. ISIJ Int. 2008;48:1596–602.
17. Porter DA, Easterling KE. Phase transformations in metals and alloys. 2nd ed. London: Chapman & Hall; 1992. p. 214.